Supporting Information

Mitigating Volume Expansion and Enhancing Cycling Stability of Ferrous Fluosilicate-Modified Silicon-Based Composite Anodes for Lithium-Ion Batteries

Jichang Sun,[1,3] Xiaoyi Liu,[1] Penglun Zheng,[3*] Yang Zhao,[4] Yun Zheng,[1*] Jingchao Chai,[1] and Zhihong Liu[2*]

[1] School of Optoelectronic Materials and Technology, Jianghan University, Wuhan 430056, P. R. China.

[2] State Key Laboratory of Precision Blasting, Jianghan University, Wuhan 430056, P. R. China.

[3] College of Civil Aviation Safety Engineering, Civil Aviation Flight University of China, Guanghan 618307, P.R. China.

[4] China Institute of Ocean Engineering (Tsing Tao), Qingdao 266555, P. R. China.

*Email: zhengyun@jhun.edu.cn (Y. Zheng); zhengpenglun@cafuc.edu.cn (P. Zheng); liuzh@jhun.edu.cn (Z. Liu)

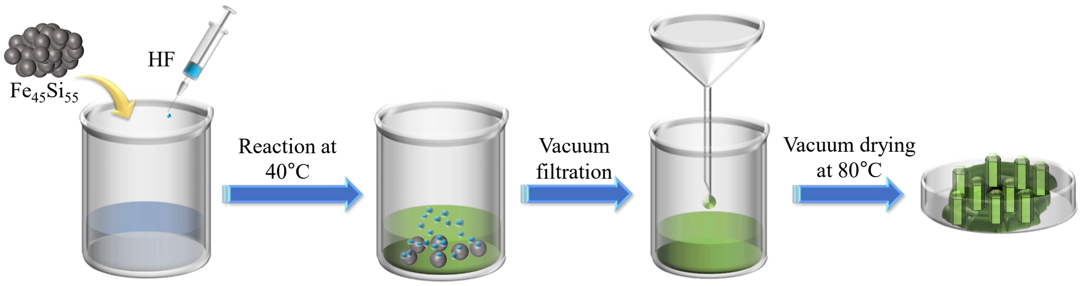

Fig. S1. Schematic illustration for the preparation of $FeSiF_6$.

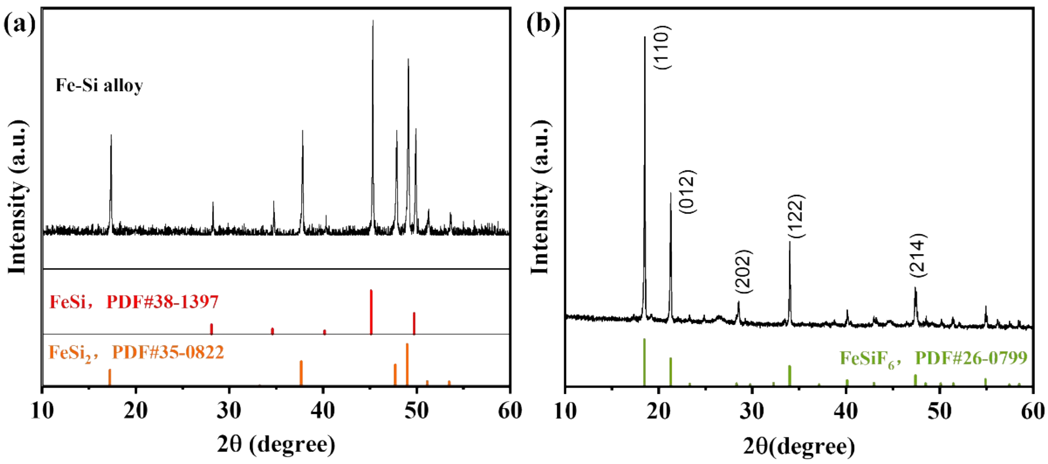

Fig. S2. XRD results of (a) $Fe_{45}Si_{55}$ and (b) as-synthesized $FeSiF_6$ composites.

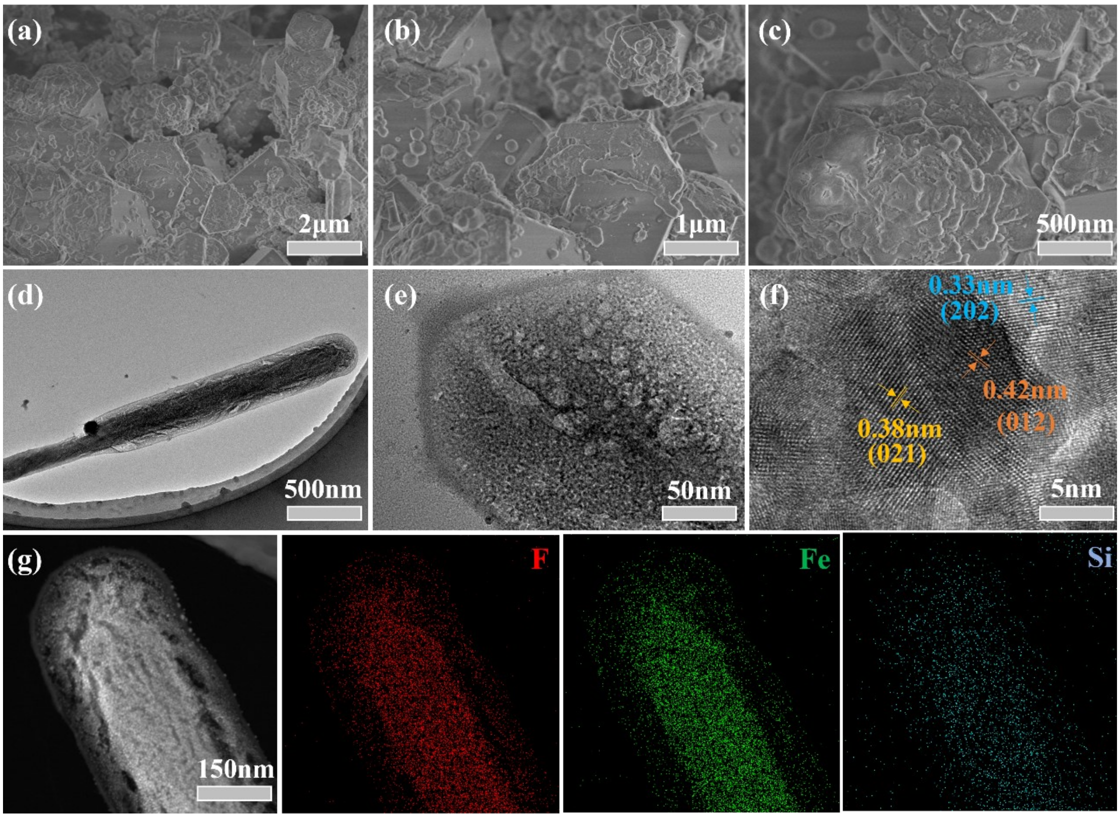

Fig. S3. (a)-(c) SEM images of pristine $FeSiF_6$ crystals. (d)-(e) TEM images of pristine $FeSiF_6$ crystals. (f) Inverse FFT image of which shows (202), (012) and (021) lattice planes of $FeSiF_6$.(e) HAADF-STEM image of a single $FeSiF_6$ wire, (f-h) The corresponding elemental mapping results of F, Fe and Si.

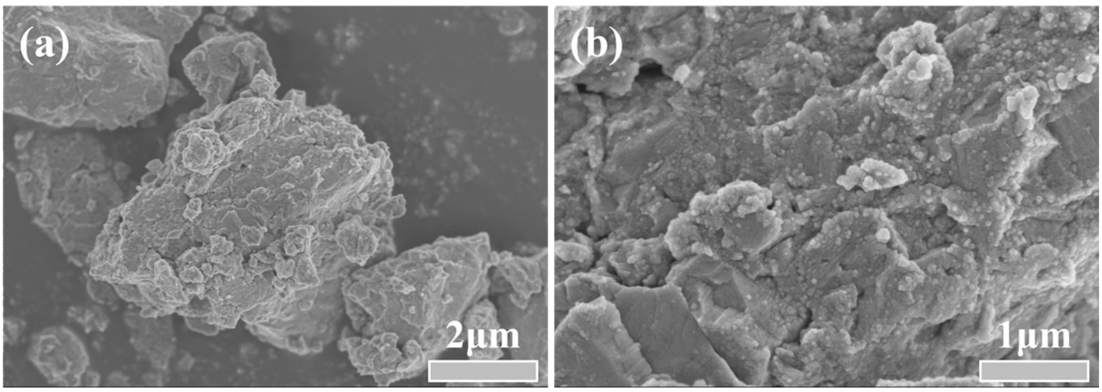

Fig. S4. (a)-(b) SEM images of pristine $Fe_{45}Si_{55}$ crystals.

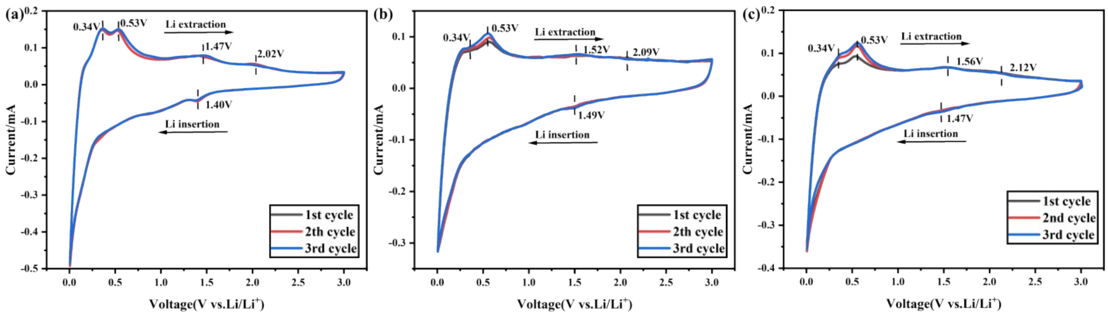

Fig. S5. Cyclic voltammetry profiles of (a) Fe-Si@C-T, (b) Fe-Si-T@C and (c) Fe-Si@F@C electrodes at a sweep rate of 0.5 mV s^{-1}.

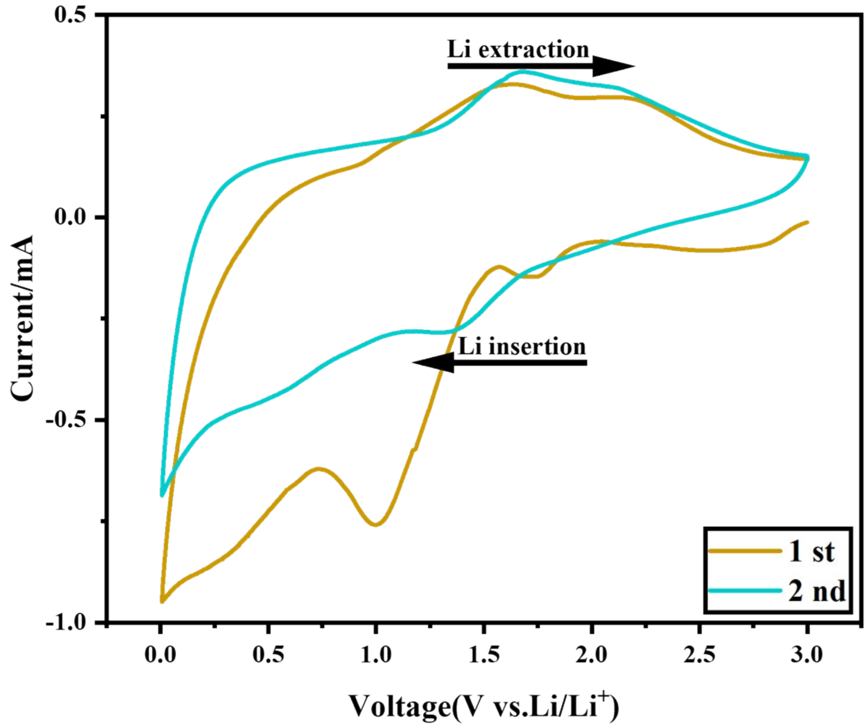

Fig. S6. Cyclic voltammetry profiles of $FeSiF_6$ composite anode in the initial five cycles at a sweep rate of 0.1 mV/s.

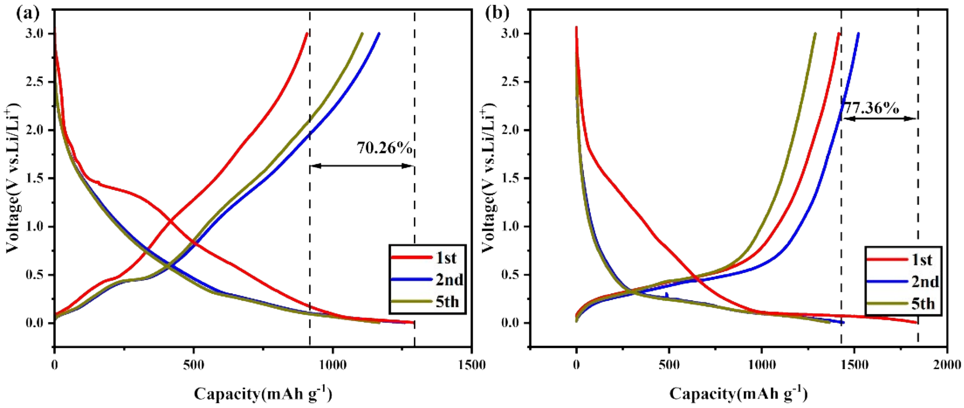

Fig. S7. Galvanostatic charge-discharge curves of (a) Fe-Si@C-T and (b) Fe-Si-T@C.

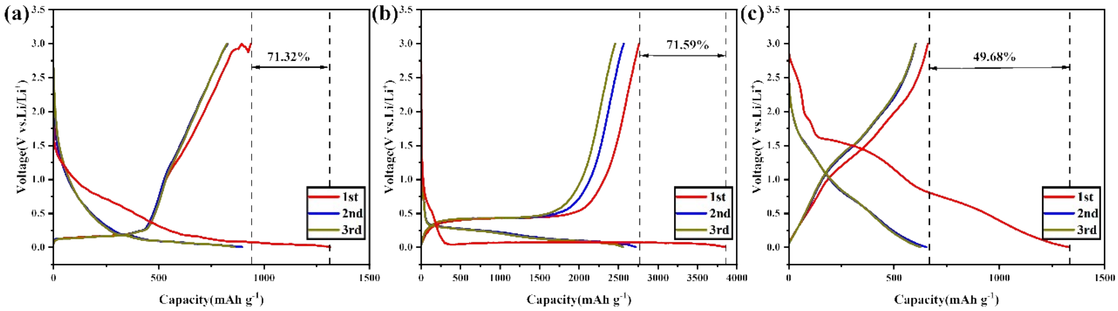

Fig. S8. GCD curves of (a) graphite (b) Si and (c) $FeSiF_6$ in the 1st, 2nd and 3rd cycles measured at 0.1A g^{-1}.

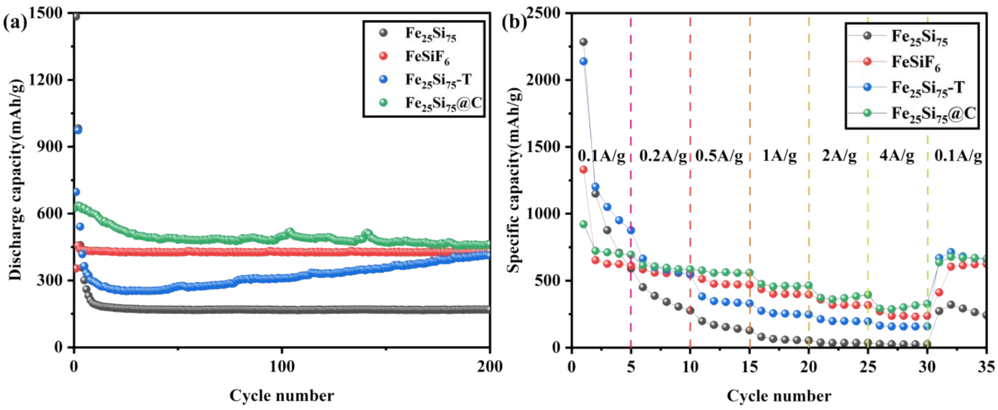

Fig. S9. (a) Cycling performance of $Fe_{25}Si_{75}$, $FeSiF_6$, $Fe_{25}Si_{75}$-T, and $Fe_{25}Si_{75}$@C at a current density of 1 A/g and corresponding fit curves. (b) Rate performance of $Fe_{25}Si_{75}$, $FeSiF_6$, $Fe_{25}Si_{75}$-T, and $Fe_{25}Si_{75}$@C at different current densities.

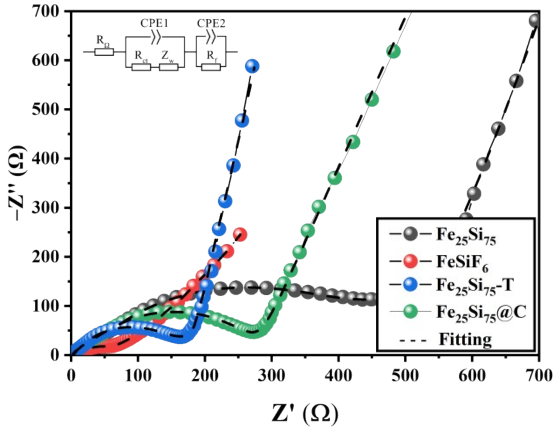

Fig. S10. EIS spectra of $Fe_{25}Si_{75}$, $FeSiF_6$, $Fe_{25}Si_{75}$-T and $Fe_{25}Si_{75}$@C with a scan rate of 0.1 mV/s. The inset shows the equivalent circuitmodel used for EIS curve fitting.

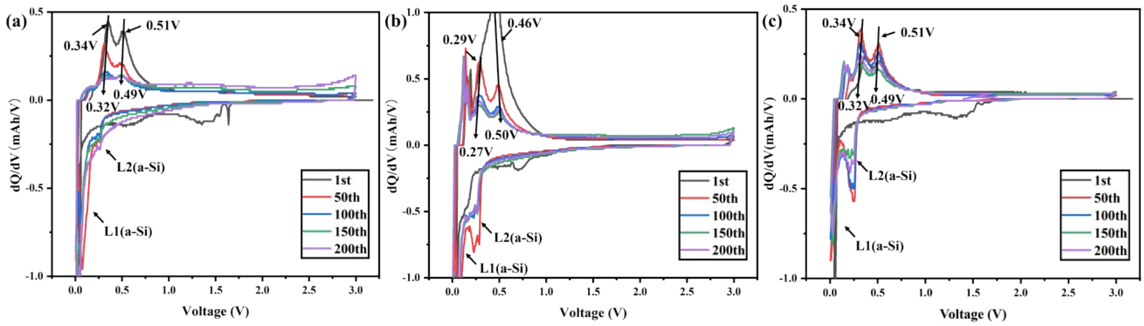

Fig. S11. The differential capacity curves of (a) Fe-Si@C-T, (b) Fe-Si-T@C, and (c) Fe-Si@F@C after different cycles at 1A/g.

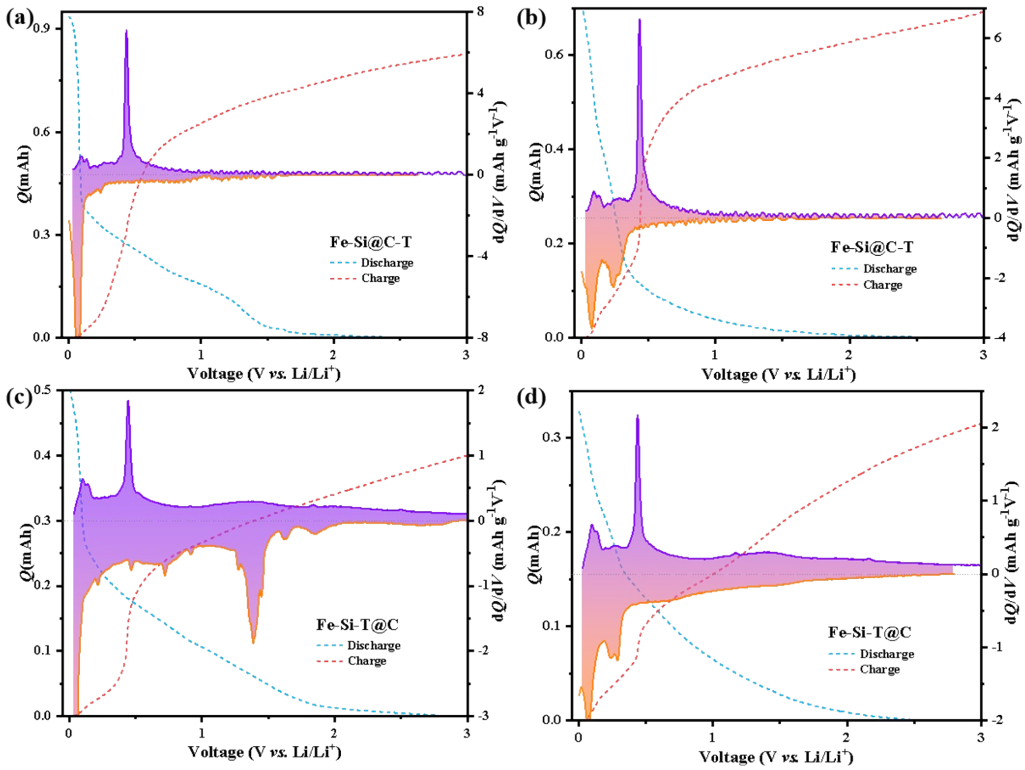

Fig. S12. Differential capacity curves for cycles of Fe-Si@C-T at (a) 1st cycle and (b) 5th cycle at 0.1A/g. (b) Differential capacity curves of Fe-Si-T@C in (a) 1st cycle and (b) 5th cycle at 0.1A/g.

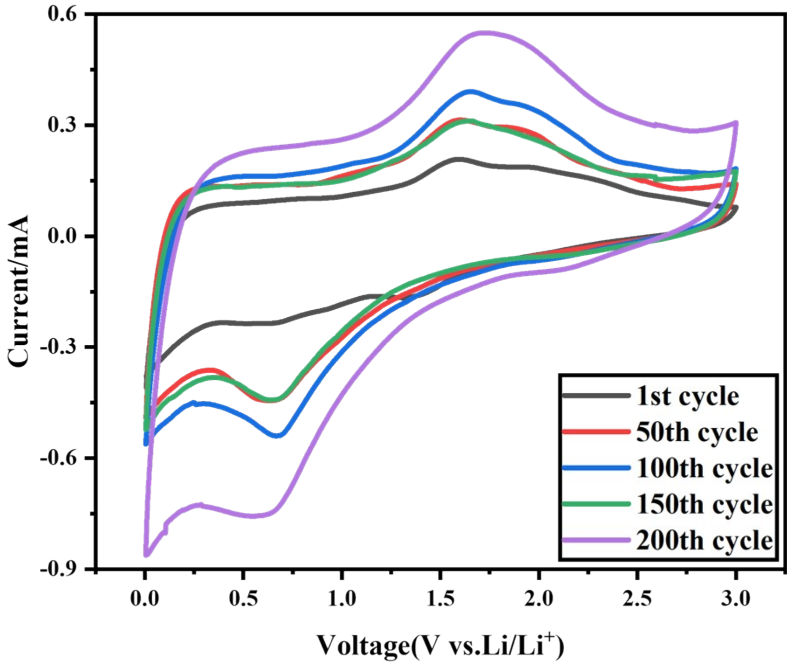

Fig. S13. Cyclic voltammetry profiles of $FeSiF_6$ anode in the initial five cycles at a sweep rate of 0.5 mV s^{-1}.

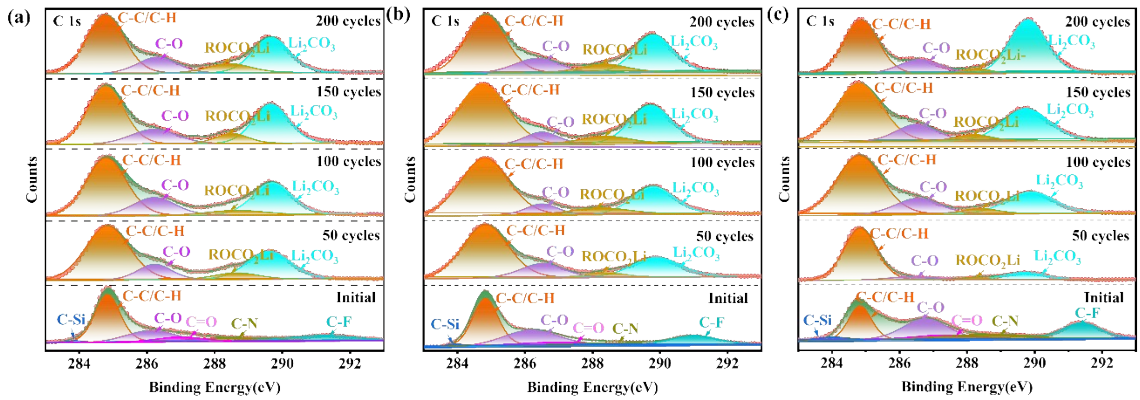

Fig. S14. High-resolution XPS spectra of C 1s of (a) $Fe_{25}Si_{75}$, (b) $FeSiF_6$, and (c) Fe-Si@F@C under different cycle times.

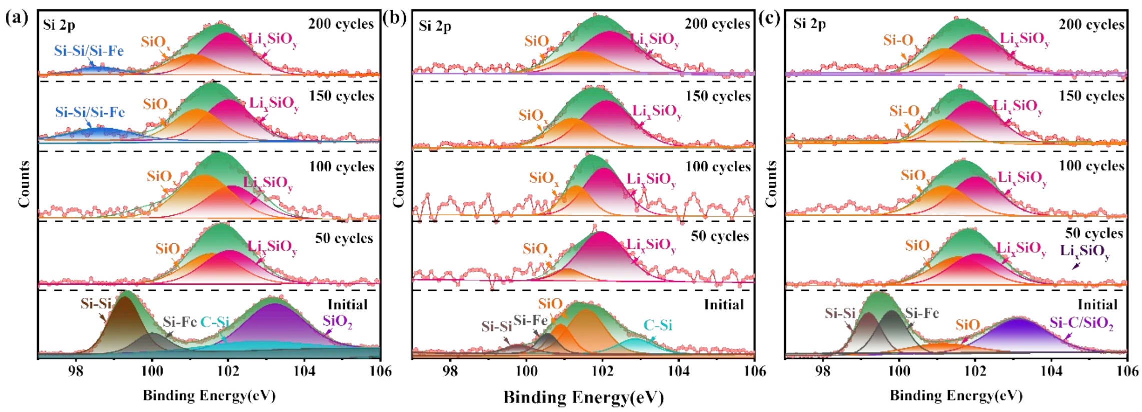

Fig. S15. High-resolution XPS spectra of Si 1s of (a) $Fe_{25}Si_{75}$, (b) $FeSiF_6$, and (c) Fe-Si@F@C under different cycle times.

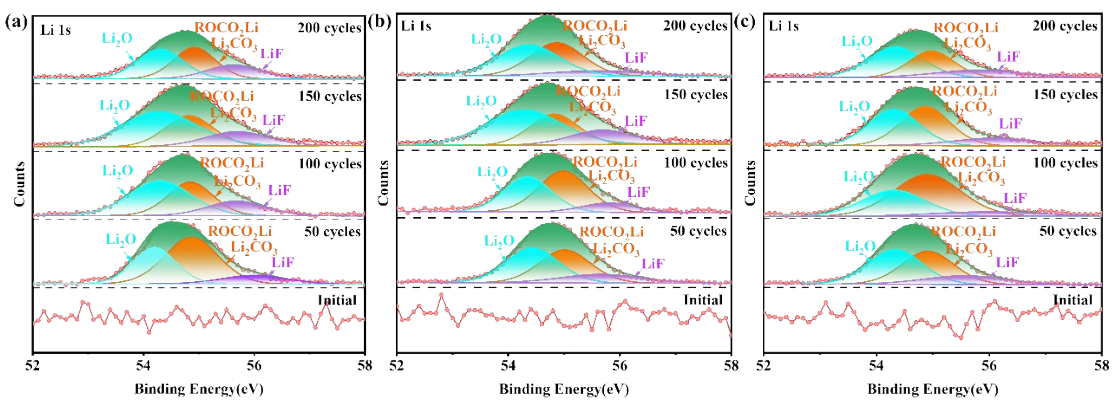

Fig. S16. High-resolution XPS spectra of Li 1s of (a) $Fe_{25}Si_{75}$, (b) $FeSiF_6$, and (c) Fe-Si@F@C under different cycle times.

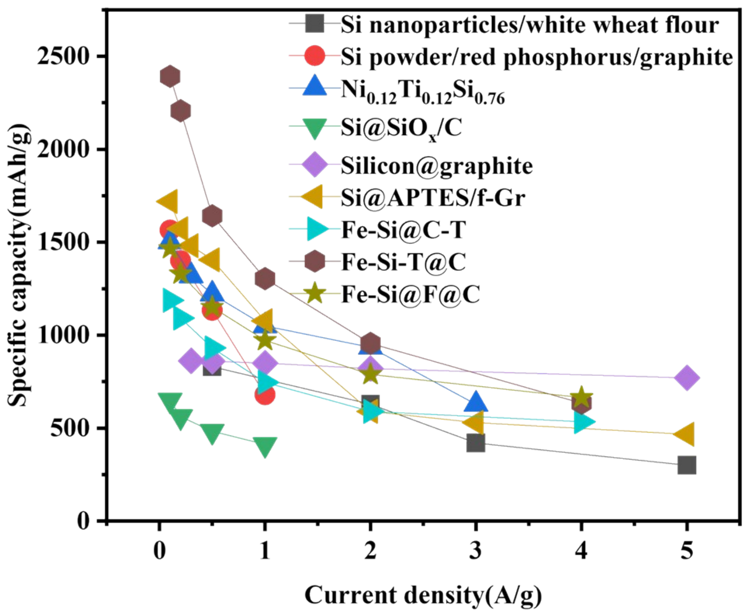

Fig. S17. Comparison of specific capacities of Fe-Si@C-T, Fe-Si-T@C, Fe-Si@F@C (this study), and other silicon-based composite anodes in literature.

Table S1. Performance comparison of silicon-based composite anodes.

Materials	Synthetic method	Synthetic method	Initial CE (%)	Anode performance	Rate	Reference
Si nanoparticles/white wheat flour	Ball milling and annealing	Core shell	71	880 mAh g^{-1} 92% retention after 90 cycles	210 mA g^{-1}	1
Si powder/red phosphorus/graphite	Ball milling	Core shell	64.7	883.4 mAh g^{-1} after 200 cycles	200 mA g^{-1}	2
Micronized Si/citric acid	Ball milling and carbonization	Core shell	82	850 mAh g^{-1} after 100 cycles	210 mA g^{-1}	3
Amorphous-$Si@SiO_x/C$	Ball milling and carbonization of the citric acid	Core shell	82	1230 mAh g^{-1} after 100 cycles	500 mA g^{-1}	4
N-doped carbon embedding Si nanoparticles	ball milling and pyrolysis carbonization	Core shell	80.8	794.7 mAh g^{-1} after 1000 cycles	1 A g^{-1}	5
$Ni_{0.12}Ti_{0.12}Si_{0.76}$	One-step ball-milling method	The ternary compound	81.8	500 mAh g^{-1} after 50 cycles	840 mA g^{-1}	6
$Si@SiO_x/C$	Two-step ball-milling	Core shell	82	726 mAh g^{-1} after 500 cycles	100 mA g^{-1}	7
Silicon@graphite	a facile and scalableball milling	Core shell	77	646.5 mAh g^{-1} after 100 cycles	200 mA g^{-1}	8

References

[1] TANG J, DYSART A D, KIM D H, et al. Fabrication of carbon/silicon composite as lithium-ion anode with enhanced cycling stability. Electrochimica Acta, 2017, 247: 626-633.

[2] HUANG S, CHEONG L-Z, WANG D, et al. Nanostructured phosphorus doped silicon/graphite composite as anode for high-performance lithium-ion batteries. ACS Applied Materials & Interfaces, 2017, 9(28): 23672-23678.

[3] KOBAYASHI N, INDEN Y, ENDO M. Silicon/soft-carbon nanohybrid material with low expansion for high capacity and long cycle life lithium-ion battery. Journal of Power Sources, 2016, 326: 235-241.

[4] WANG D, GAO M, PAN H, et al. High performance amorphous-Si@ SiO_x/C composite anode materials for Li-ion batteries derived from ball-milling and in situ carbonization. Journal of Power Sources, 2014, 256: 190-199.

[5] HAN J, ZHAO C, WANG L, et al. Simple ball milling-assisted method enabling N-doped carbon embedded Si for high performance lithium-ion battery anode. Journal of Alloys and Compounds, 2023, 966: 171668.

[6] LADAM A, BIBENT N, CéNAC-MORTHé C, et al. One-pot ball-milling synthesis of a Ni-Ti-Si based composite as anode material for Li-ion batteries. Electrochimica Acta, 2017, 245: 497-504.

[7] QIAN L, LAN J-L, XUE M, et al. Two-step ball-milling synthesis of a Si/SiO_x/C composite electrode for lithium ion batteries with excellent long-term cycling stability. RSC Advances, 2017, 7(58): 36697-36704.

[8] CABELLO M, GUCCIARDI E, HERRáN A, et al. Towards a high-power Si@ graphite anode for lithium ion batteries through a wet ball milling process. Molecules, 2020, 25(11): 2494.